ACS OMEGA

Open Access

http://pubs.acs.org/journal/acsodf

Article

Development of a Crystallographic Screening to Identify Sudan Virus VP40 Ligands

Anke-Dorothee Werner, Nils Krapoth, Michael J. Norris, Andreas Heine, Gerhard Klebe, Erica Ollmann Saphire, and Stephan Becker*

Cite This: *ACS Omega* 2024, 9, 33193−33203

Read Online

ACCESS | Metrics & More | Article Recommendations | Supporting Information

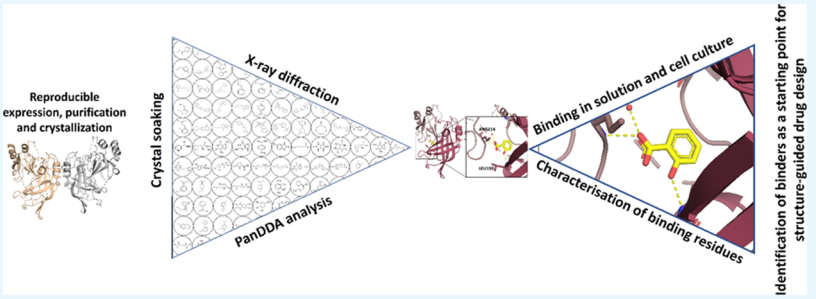

ABSTRACT: The matrix protein VP40 of the highly pathogenic Sudan virus (genus *Orthoebolavirus*) is a multifunctional protein responsible for the recruitment of viral nucleocapsids to the plasma membrane and the budding of infectious virions. In addition to its role in assembly, VP40 also downregulates viral genome replication and transcription. VP40's existence in various homo-oligomeric states is presumed to underpin its diverse functional capabilities during the viral life cycle. Given the absence of licensed therapeutics targeting the Sudan virus, our study focused on inhibiting VP40 dimers, the structural precursors to critical higher-order oligomers, as a novel antiviral strategy. We have established a crystallographic screening pipeline for the identification of small-molecule fragments capable of binding to VP40. Dimeric VP40 of the Sudan virus was recombinantly expressed in bacteria, purified, crystallized, and soaked in a solution of 96 different preselected fragments. Salicylic acid was identified as a crystallographic hit with clear electron density in the pocket between the N- and the C-termini of the VP40 dimer. The binding interaction is predominantly coordinated by amino acid residues leucine 158 (L158) and arginine 214 (R214), which are key in stabilizing salicylic acid within the binding pocket. While salicylic acid displayed minimal impact on the functional aspects of VP40, we delved deeper into characterizing the druggability of the identified binding pocket. We analyzed the influence of residues L158 and R214 on the formation of virus-like particles and viral RNA synthesis. Site-directed mutagenesis of these residues to alanine markedly affected both VP40's budding activity and its effect on viral RNA synthesis, underscoring the potential of the salicylic acid binding pocket as a drug target. In summary, our findings lay the foundation for structure-guided drug design to provide lead compounds against Sudan virus VP40.

1. IMPORTANCE

Ebola virus causes severe fever with unusually high case fatality rates, which can only be treated symptomatically, as there are no therapeutics available. VP40 plays a key role in the viral replication process, as it promotes the budding of new virions and is also involved in the regulation of viral genome replication and transcription. While VP40 of the Ebola virus has been characterized in depth, hardly any work has been done on VP40 of the Sudan virus, another highly pathogenic species within the genus *Orthoebolavirus* in the family of *Filoviridae*. The recent outbreak of the Sudan virus in Uganda, however, emphasizes the need for the development of new antivirals. Here, fragment-based lead discovery was employed to identify VP40-binding small molecules that could serve as promising lead or lead-like structures during structure-guided drug design with the goal of developing a potent VP40 inhibitor.

2. INTRODUCTION

The genus *Orthoebolavirus* within the family of *Filoviridae* in the order *Mononegavirales* comprises six species. Among them, Ebola virus (*Orthoebolavirus zairense*, EBOV), Bundibugyo virus (*Orthoebolavirus bundibugyoense*), and Sudan virus

Received: May 22, 2024
Revised: July 5, 2024
Accepted: July 5, 2024
Published: July 18, 2024

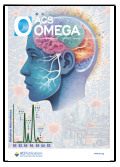

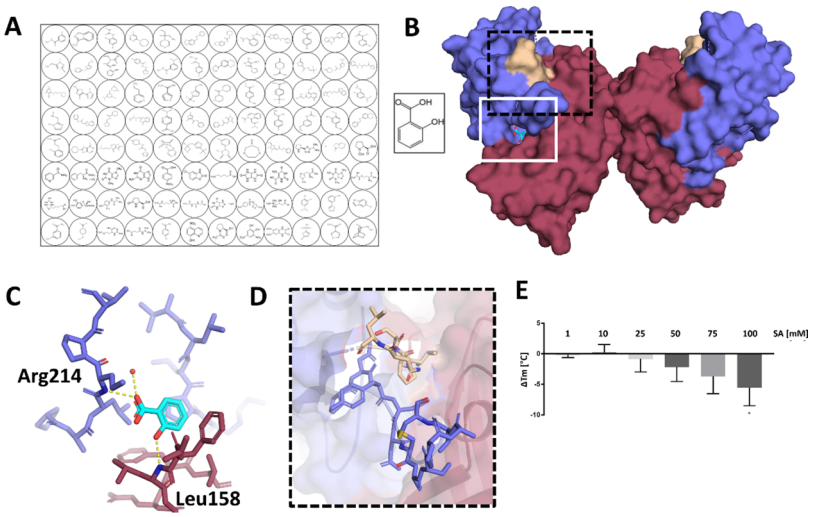

Figure 1. Salicylic acid of the Jena FragXtal Screen was identified as a sVP40-binder. (A) Composition of the Jena FragXtal Screen. (B) sVP40 WT (PDB-ID 8B2U) in surface representation with the NTD (dark red) and the CTD (blue). The binding site of SA (white box, formula, boxed rectangle), linker, and C-terminal arm (black box) are shown in panels C and D, respectively. (C) Close-up of the SA binding pocket (SA shown in cyan) between NTD and CTD with H-bonds to Leu158, Arg214 (not all atoms of the side chains were modeled), and a water molecule. (D) A close-up of the linker (wheat) and C-terminal arm (blue) shown in the stick representation, with the remaining part of the structure shown as both cartoon and surface (transparency 60%). (E) Thermal stability of sVP40 in complex with SA. Means of denaturing temperatures upon incubation with increasing concentrations of SA (1−100 mM) were compared with apo $sVP40_{\Delta 43}$ WT (three independent experiments).

(*Orthoebolavirus sudanense*, SUDV) are the most pathogenic with unusually high case fatality rates.[1,2] While vaccines and monoclonal antibody cocktails are available against EBOV and are being used during outbreaks,[3,4] much-needed small-molecule drugs as well as therapeutics are missing, especially against SUDV,[5] the causative agent of the most recent filovirus outbreak in Uganda.[6,7]

VP40 is the *ebolavirus* matrix protein, which forms different oligomers that have distinct functions in the viral replication cycle.[8] VP40's N-terminal domain (NTD; residues 1−194) is connected to its C-terminal domain (CTD; residues 201−326) via a flexible linker, which allows movement between the NTD and CTD.[9] The CTD mediates the binding of VP40 to cellular membranes.[10] VP40 exhibits a high degree of sequence and structural similarity between the different *Orthoebolavirus* species (Figures S1 and S2). Dimeric VP40 adopts a butterfly shape, and the two protomers are joined via residues 52−65 and 108−117 of the NTD. VP40 dimers can be transported to the plasma membrane along cellular membranes.[8,11] At the plasma membrane, VP40 dimers are triggered by contact with phosphatidylserine to homo-oligomerize into filaments,[12] in which the dimers are connected through their CTD with residues L203, I237, M241, M305, and l307. Budding is then facilitated upon the interaction of VP40 with the COPII transport system[13] and the endosomal complexes required for transport (ESCRT) complex; the interaction with the latter is enabled by VP40's two late budding domain (L domains) motifs 7-PTAP-10 and 10-PPxY-13.[14] The third homo-oligomeric form of VP40 is an octameric ring assembly.[15] A recent study has shown that dimeric VP40 can be triggered into the octamer upon incubation with certain DNA or RNA.[16] The octameric structure also includes the triribonucleotide 5′-UGA-3′ that is bound to residues R134 and F125 of each monomer.[8,15] Octameric VP40 was reported to be involved in the downregulation of viral genome replication and transcription, although the details remain unclear.[8,17,18] In order to identify VP40-directed inhibitors, various functions of VP40 were targeted, including dimerization and transport[19,20] or interaction with the plasma membrane, egress, or filament formation.[21,22]

Fragment-based drug discovery or fragment-based lead design has become a widely used approach to identify molecular binders that can be developed into promising inhibitors.[23] This highly sensitive method involves soaking crystals of the target protein with a series of low-molecular-weight fragments and subsequent analysis of the crystals at a beamline. This experimental setup detects even weak binders.[24] Another advantage is the gained structural information showing how and where the fragment binds to the protein.[25] Due to the low number of atoms and functional groups of fragments, they represent promising starting points for the development of larger lead structures, therefore necessitating only a small library for screening.

Here, we present the first structure-based lead discovery addressing SUDV matrix protein VP40 by using a crystal soaking pipeline. We identified salicylic acid as a binder in both the crystalline state as well as in solution. While salicylic acid displayed a minimal impact on the functional aspects of VP40, we confirmed the binding pocket to be a promising drug target.

3. RESULTS

3.1. Crystallographic Fragment Screening Yields Salicylic Acid as a Hit. Expression, purification, and crystallization of truncated SUDV VP40 lacking the first 43 N-terminal amino acids ($sVP40_{\Delta 43}$) were optimized to reproducibly achieve crystals of dimeric $sVP40_{\Delta 43}$ that diffract better than 2 Å.[26] For the crystal soaking, the Jena FragXtal Screen was used.[27,28] This library consists of 96 fragments (J1−J96; Figure 1A), mostly adhering to the Astex rule of three (Ro3).[29,30] This rule is based on Lipinski's rule of five (Ro5),[31] describing the chemical properties for oral availability of drug-like molecules or drug candidates. For Astex Ro3, fragments obey limitations such as molecular weight ≤300 Da and number of hydrogen bond donors and acceptors ≤3.[32] This

https://doi.org/10.1021/acsomega.4c04829
ACS Omega 2024, 9, 33193−33203

library was already used for a number of screening analyses.[27,28,33,34] All fragments were dissolved in dimethylsulfoxide (DMSO) and diluted in crystallization buffer to 100 mM (final concentration of 10% v/v). One or several crystals were then soaked with each fragment for 12−16 h, 1 h or 10 s, flash-frozen, and analyzed via X-ray diffraction. In total, 140 data sets, including negative controls soaked only in 10% DMSO, were collected and analyzed via the *PanDDA* suite,[35] and the autorefinement pipeline, which was developed by Schiebel et al.[30] Positive electron density could be observed for crystals soaked with fragment J15 (salicylic acid (SA) mixed with *N*,*N*-diethylethanimidamide in a 1:1 ratio). Of the two fragments, only SA could be detected in the electron density map of $VP40_{\Delta 43}$ (Figure 1B,C, Table 1, PDB-ID 8B2U). SA occupied

Table 1. Data Collection and Refinement Statistics of Dimeric $sVP40_{\Delta 43}$ WT in Complex with SA[a]

data collection	8B2U (soaking)	8B1S (cocrystallization)
space group	*C*2	*C*2
unit cell parameters [Å] (*a*, *b*, *c*, *α*, *β*, *γ*)	62.30; 90.62; 48.10 90.00; 94.02; 90.00	62.10; 90.62; 48.19 90.00; 94.25; 90.00
resolution range	47.99−1.80 (1.84−1.80)	48.06−1.60 (1.63−1.60)
total number of reflections	81,399 (4,329)	233,261 (9,242)
number of unique reflections	24,102 (1,315)	33,883 (1,474)
I/σ	6.4 (0.7)	21.8 (3.8)
R_{merge}	0.076 (1.020)	0.037 (0.318)
completeness [%]	97.9 (90.4)	97.7 (86.7)
multiplicity	3.4 (3.3)	6.9 (6.3)
$CC_{1/2}$ [%]	99.5 (42.4)	99.9 (97.2)
	Refinement	
resolution range	47.99−1.80	36.14−1.60
R_{work}/R_{free} [%]	20.8/23.0	18.9/20.7
number of unique reflections	23.796	33,841
number of protein residues	248	244
average *B* factor [Å^2]	43.5	37.0
r.m.s deviations:		
bond length [Å^2]	0.007	0.004
bond angles [deg]	0.91	0.73
Ramachandran plot:		
favored [%]	97.88	98.26
allowed [%]	2.12	1.74
outliers [%]	0.00	0.00
rotamer outliers [%]	0.00	0.00
clash score	1.88	3.19
number of TLS groups	5	5

[a]Values for the outer shell are given in parentheses.

the pocket between the NTD and CTD and formed H-bonds to the backbones of L158 (NTD), R214 (CTD), and a water molecule (Figure 1B,C). The side chain of sVP40 R214 did not have clear electron density and was only partially modeled in the final pdb-model (Figure 1C). Interestingly, this structure revealed features that we characterized in a previous study, such as the very end of the C-terminus, including the only two cysteines of VP40 connected via a disulfide bridge, as well as the linker between the NTD and CTD (Figure 1B,D (PDB-ID 8B3X)).[26]

To ensure soaking of SA in the crystalline state did not introduce a bias into the interaction mode, we cocrystallized VP40 with SA.[36,37] This approach revealed the same binding mode and position of SA as those during the soaking experiments (Table 1, PDB-ID 8B1S, Figure S3). The binding of SA to sVP40 in solution was confirmed using a thermal shift assay (TSA). Incubation with sodium salicylate decreased VP40's thermal stability in a dose-dependent manner (Figures 1E and S4).

3.2. Salicylic Acid Showed Minor Effects on VP40's Functions. As a next step, we investigated whether the binding of SA impaired VP40's functions. First, an EBOV-based minigenome (MG) assay was used to analyze the function of sVP40, as a SUDV-based MG assay was not available. For this, HEK293 cells were transfected with the MG components[38] and a plasmid encoding sVP40 and treated with increasing concentrations of SA. Reporter gene activity was measured at 48 h post-transfection (p.t.). As anticipated, wild-type sVP40 (sVP40 WT) inhibited reporter gene expression in a dose-dependent manner. To achieve reporter gene activity reduction comparable to that observed with EBOV VP40 (eVP40), a higher quantity of the sVP40-encoding plasmid was required for transfection (Figure S5). Treatment with 1 mM SA impacted reporter levels even further, whereas they were slightly increased upon incubation with 10 μM SA compared to that of the untreated VP40 sample (Figure 2A).

To investigate the potential inhibitory effect of SA on the release of VP40, a budding assay was performed. HEK293 cells were transfected with plasmids encoding sVP40 and the viral glycoprotein (GP), the latter to increase the yield of virus-like particles (VLPs), and treated with SA for 4 h p.t. The ratio of released/intracellular VP40 was determined via Western blotting. VP40 release was not significantly impaired by any of the SA concentrations used (Figure 2B,C). Because MG and VLP assays represent artificial overexpression systems to study the distinct steps of the viral replication cycle, a potential inhibitory effect of SA on authentic SUDV was tested under the BSL4 conditions. For this, HuH7 cells were infected with SUDV at an MOI of 0.01 and treated with increasing concentrations of SA. As shown in Figure 2D, SA treatment had no significant effect on released viral titers.

Taken together, SA seemed to exert only slight changes in reporter gene activity in an MG assay and had no implications for budding. Because SA covers only a small fraction of the large binding pocket, this result was not unexpected.

3.3. Characterization of Residues Involved in the Interaction of SA with VP40. To investigate the biological relevance of the SA binding pocket and therefore its suitability as a drug target to inhibit functions of VP40, we characterized the residues that are involved in the interaction with SA, L158, and R214 and also included L213. The mutants sVP40 L158A, sVP40 L213A, and sVP40 R214A were generated in the mammalian expression vector pCAGGS and used in MG and budding assays. As shown in Figure 3A, the inhibitory effect of VP40 on viral genome replication and transcription was completely abolished upon mutation of R214. In addition, a slight but not significant effect was observed for sVP40 L158A.

Next, we examined the same set of mutants within a VLP assay, which revealed that each of the mutated amino acids played a critical role in the initiation of VLPs. Notably, the mutations markedly reduced the efficiency of budding, with the most pronounced decrease observed for the sVP40 L213A mutant (Figure 3B,C). These findings are consistent with the existing literature; specifically, residues L213 and R214 have been previously investigated in the context of eVP40.[39,40] A recent study highlighted the importance of electrostatics of the linker residues between the NTD and CTD for the interaction

https://doi.org/10.1021/acsomega.4c04829
ACS Omega 2024, 9, 33193−33203

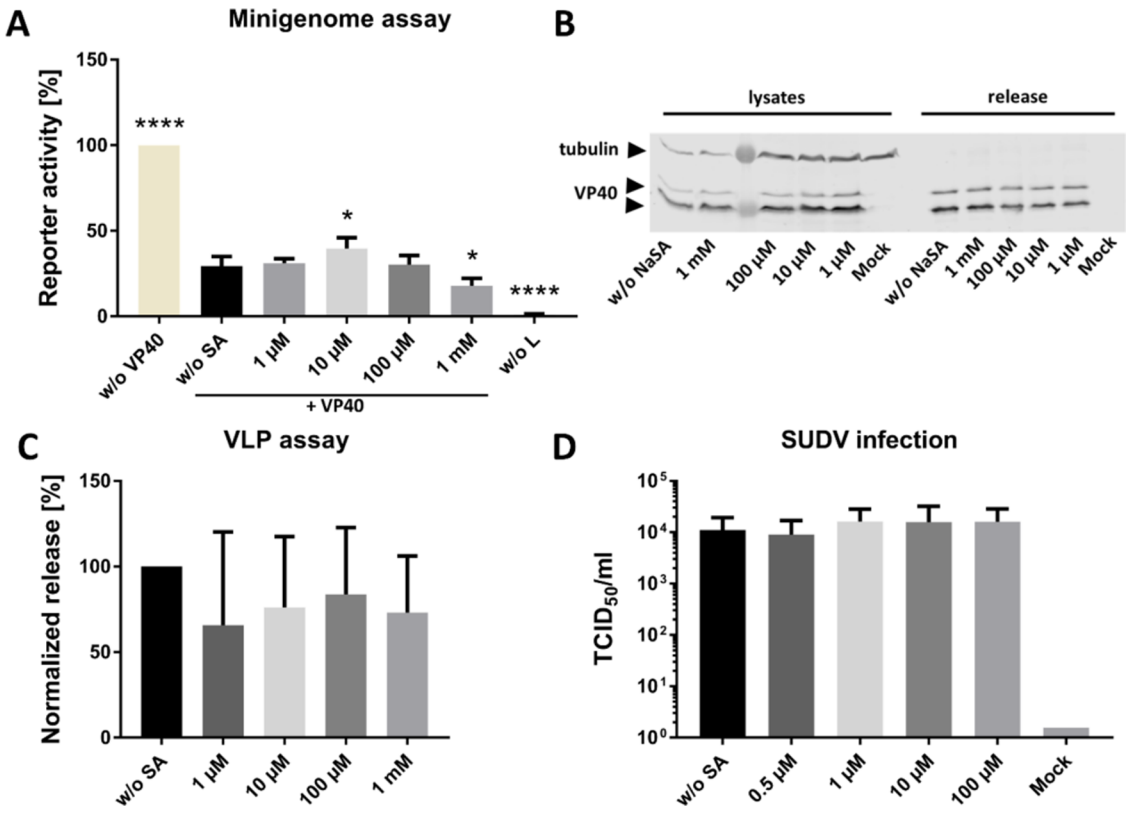

Figure 2. SA displays only minor effects on VP40 in functional assays. (A) Treatment with SA influences reporter gene activity in a minigenome assay. HEK293 cells were transfected with pCAGGS sVP40 WT and the minigenome assay components. The cell culture medium was changed 4 h p.t., and increasing concentrations of SA were added (1 μM−1 mM). Cells were lysed 48 h p.t., and reporter gene activity was measured and normalized to the sample without VP40 (set to 100%). For the negative control, no polymerase L was added to the transfection mix. (B, C) The effect of SA treatment on VP40 release. Cells were transfected with pCAGGS GP and pCAGGS sVP40 WT, and the cell culture medium was changed 4 h p.t., and SA added. Supernatants were collected, and cells were lysed 24 h p.t., and Western blot analyses of cellular and released VP40 were performed using rabbit α-VP40 and mouse α-tubulin as primary antibodies and donkey α-mouse and goat α-rabbit IRDye 680 as secondary antibodies. (C) Quantification of VLPs. Released VP40 was normalized to the amount of VP40 in lysates, and sVP40 WT w/o SA was set to 100%. (D) HuH7 cells were infected with SUDV and treated with varying concentrations of SA. Viral titers of the supernatants were assessed at 2 dpi via TCID50. Bars indicate the mean ± SD of at least three independent experiments, and asterisks indicate statistical significance (*P < 0.05 and ****P < 0.0001) compared to the positive control without SA.

with the cellular plasma membrane and showed that differences in the net charge of VP40 alter budding dynamics.[41] To investigate a similar mechanism for the pocket residues, we prepared various R214 mutants and assessed their functionality in an MG and budding assay (Figure 3D,E) and could show that the net charge plays only a minor role in the regulation of viral RNA synthesis (especially when compared to R214A, Figure 3A). In contrast, defects in budding activity are more prominent for negative or uncharged substitutions compared to other substitutions that retain net charges, such as R214K or R214H (Figure 3E). Expression levels of all R214 mutants were similar (Figure S6).

To further explore the effects of these point mutations, we assessed their impact on the ability of sVP40 to form homo-oligomers. To this end, we generated mutants sVP40$_{\Delta 43}$ L158A, L213A, and R214A using the bacterial expression vector pET46. The resultant recombinant proteins were expressed in *Escherichia coli*, purified through affinity chromatography, and then analyzed by size-exclusion chromatography (SEC). The SEC analysis revealed that while the wild-type sVP40$_{\Delta 43}$ protein predominantly eluted as dimers with a detectable, albeit minor, octamer fraction, the mutant proteins demonstrated a decrease in dimer formation coupled with an increased octamer fraction (Figure 3F), as determined via calculating the area under the curve (AUC) for the different oligomeric peaks and the octameric fraction (Figure 3G). This suggested that the residues coordinating SA, particularly L158 or R214, are important for the stability of VP40 dimers. While it has been discussed that octamers of VP40 play an important role in the downregulation of RNA synthesis,[8,17] this presumption is not confirmed by our results, where R214A lost its ability to inhibit viral RNA synthesis although the amount of VP40 octamers was increased from 10 to 50% (Figure 3F,G).

In our study, we demonstrated that fragment-based drug discovery identified SA to bind with low affinity in a pocket of VP40 that is important for the protein's function. The SA-coordinating amino acids L158 (NTD) and R214 (CTD) are essential for the budding function and viral RNA synthesis-modulating function of VP40. The identified binding site on VP40 is therefore promising for the further development of SA derivatives in order to inhibit the functions of VP40's functions.

4. DISCUSSION

The recent SUDV outbreak in Uganda stresses the need for virus-specific vaccines and novel antivirals. So far, SUDV has remained mainly understudied compared to EBOV. We

https://doi.org/10.1021/acsomega.4c04829
ACS Omega 2024, 9, 33193−33203

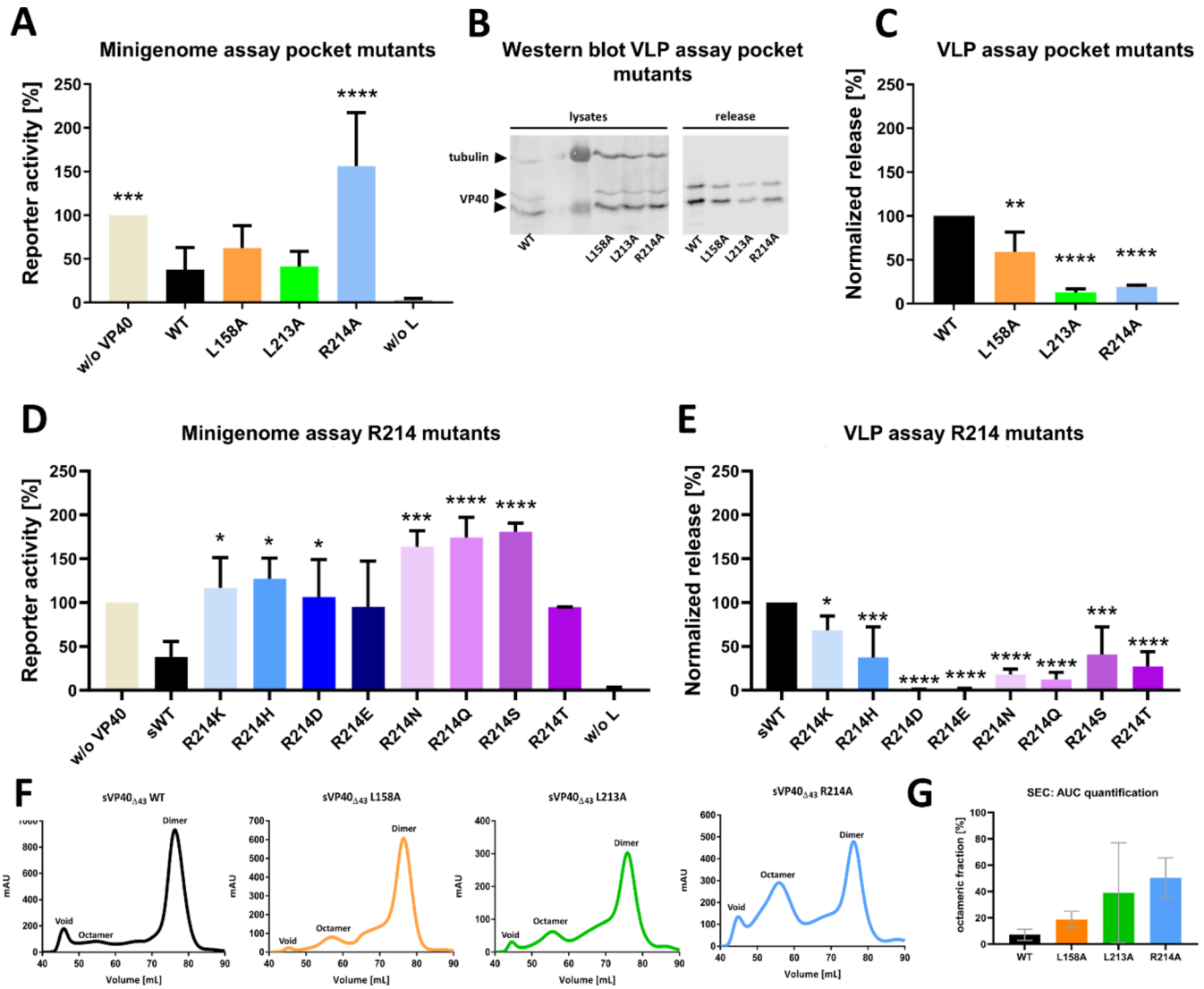

Figure 3. Influence of sVP40 pocket mutants on reporter gene activity, budding, and homo-oligomerization. (A) Influence on an MG assay: HEK293 cells were transfected with pCAGGS sVP40 WT or mutants along with the minigenome assay components. Cells were lysed 48 h p.t., and reporter gene activity was measured and normalized to the sample without VP40 (set to 100%). For the negative control, no polymerase L was added to the transfection mix. (B, C) The effect of sVP40 pocket mutants on VP40 release: cells were transfected with pCAGGS GP and sVP40 WT or mutants. Supernatants were collected, and cells lysed 24 h p.t. and Western blot analyses of cellular and released VP40 were performed using rabbit α-sVP40 and mouse α-tubulin as primary antibodies and donkey α-mouse and goat α-rabbit IRDye 680 as secondary antibodies. Quantification of VLPs: released sVP40 was normalized to the amount of sVP40 in lysates, and sVP40 WT was set to 100%. VP40 typically exhibits two major bands, both of which were used for quantification. (D) Influence of different arginine substitutions on reporter gene activity. (E) The effect of arginine substitutions on VP40 release. (F) Size-exclusion chromatography of sVP40 WT and pocket mutants. (G) Area under the curve (AUC) of the different VP40 oligomers: size-exclusion chromatography and calculation of the AUC of the dimeric and octameric peaks and determination of the octameric percentage of total VP40 AUC. Bars indicate the mean ± SD of three independent experiments, and asterisks indicate statistical significance as follows: *P < 0.05, **P < 0.005, ***P < 0.0005, and ****P < 0.00005 compared to sVP40 WT.

successfully employed fragment-based lead design via crystal soaking and identified salicylic acid as a crystallographic binder of dimeric sVP40. The success rate of the screening described here was surprisingly low, with only one fragment identified as a hit when compared to other publications using the same library.[28,34,42] Other fragments of the Jena FragXtal screen that are structurally quite similar to SA did not bind, suggesting that the functional groups are crucial for successful soaking (Table S1). Due to its small size, SA seems to be a promiscuous binder, as it was reported as a ligand for numerous other proteins,[43−52] also including screenings using the same library.[42,53] SA derivatives such as 2-hydroxy-4-aminobenzoic acid and *P*-hydroxybenzoic acid are bound to the SARS-CoV-2 NSP3 macrodomain in the crystalline state (PDB-codes: 5RUE and 5RTJ, respectively).[54]

SA was identified as a crystallographic binder in the crystal soaking screening, and its binding was confirmed in solution via TSA. The TSA results suggested a destabilization of sVP40 in its dimeric form. Decreased melting temperatures upon ligand binding was reported previously for other proteins.[55−57] However, the sVP40 crystal in complex with SA did not exhibit altered topology compared to the apo form (PDB-code 8B3X,[26] (Figure S3)), as indicated by a root-mean-square deviation (RMSD) of 0.144 for 8B2U vs 8B1S and 0.140 and 0.166 for 8B3X vs 8B2U and 8B1S, respectively. The characterization of the pocket mutants sVP40 L158A,

https://doi.org/10.1021/acsomega.4c04829
ACS Omega 2024, 9, 33193−33203

L213A, and R214A showed that VLP formation of the mutants is impaired concomitant with an increase in the octameric fraction compared to sVP40 WT (Figure 3F,G). The increased formation of octamers might represent a destabilization of dimeric VP40, which could account for the destabilizing effect seen in the TSA. It might also explain the decrease in budding activity, which is in line with the literature described for eVP40 L213A and R214A.[39] Additionally, L213 was reported to penetrate into the plasma membrane, along with I293, L295, and V298,[40] and the eVP40 L213A mutant exhibited decreased plasma membrane localization and penetration as well as diminished externalization of phosphatidylserine on the outer leaflet of the plasma membrane,[12] which promotes efficient uptake of virions by target cells.[58] The abrogated interaction with the plasma membrane might be another reason for decreased levels of VP40 in the cell culture supernatant. Also, similar implications are possible for R214 as this residue is located on the outer rim of the pocket. Therefore, two scenarios are imaginable: First, it can be suggested that SA binding induces a possible destabilization of the sVP40 by directly affecting the pocket and its residues. However, our experimental TSA data shows that while the dimer is indeed affected, its destabilization is not severe enough to impair the dimerization, as evidenced by the absence of a monomeric peak (see Figure S4) in the melt curve. Second, a stabilization of the dimer is also conceivable since SA forms interactions with both termini and thus could possibly interfere with octamerization, which involves a conformational rearrangement of the CTD. Other possibilities upon binding of pocket-directed inhibitors include impaired function of VP40 due to the blockade of the crucial residues L158, L213, and R214, which could impair interaction with other viral or host proteins due to the occupied pocket. All possibilities, however, depend on the development of a (larger) SA derivative that binds to VP40 with a higher affinity.

While the overall topology of the SA binding pocket is highly conserved among the different ebolavirus species (Figure S2), the cavity is occupied by the very end of the C-terminal domain in the eVP40 structure as well as in the models generated using ColabFold.[59] However, the terminal arm seems to necessitate a high level of flexibility, suggesting that a ligand such as SA can bind to VP40 depending on the conformational state or might even be able to displace the C-terminal arm. The characterized area represents the only pocket of dimeric VP40 besides a shallow tunnel formed by residues 67−70, 102−105, and 273−280 on top of the dimer. Urata et al. hypothesized that the pocket between the CTD and NTD is the interaction site between VP40 and other viral or host proteins, such as NP[60] or proteins of the COPII transport system,[13] but so far, involved residues or structure remained enigmatic. Urata et al. characterized the 292-YIGL-295 motif for eVP40, which is located inside the pocket and was reported to be critical for both VLP release and downregulation of viral genome replication and transcription.[61] This further increases the attractiveness of the pocket and also raises questions about its accessibility. In this regard, it needs to be mentioned that accessibility is given due to the flexibility of the R214 side chain, which could not be completely modeled in any of the $sVP40_{\Delta 43}$ WT structures of the present study. Generating the symmetry mates of the crystal packing showed that the pocket is still solvent-exposed and not blocked by other protomers in the crystal, whereas other areas are obstructed (Figure S7).

Identification of antivirals against filoviruses typically included high-throughput screenings using relatively large libraries and complex molecules.[19,62−65] Due to their size, these compounds are potentially highly potent but are often unspecific binders and tend to have high off-target effects. In addition, they usually offer only reduced chemical diversity, making modification more challenging. On the other hand, fragments are ideally suited for purpose- and target-specific modification and are therefore attractive for the drug discovery process. However, fragments typically exhibit weak binding affinities in the millimolar range and, therefore, require highly sensitive screening methods. Extension of hits into lead compounds requires the synthesis of a potentially extensive array of molecules until a suitably potent compound emerges. This process becomes exponentially intricate in the absence of structural information as the number of synthesized molecules is potentially dramatically increased at each step of the development (reviewed in refs 66−68). While the implementation of crystal soaking experiments proved labor-intensive in the initial phases, structure-guided drug design is greatly facilitated. This, in turn, substantially mitigates the challenges associated with the design and synthesis of derivatives as possible extension sites are easily located and validated using our approach.

In conclusion, a crystal soaking screening is a powerful technique to identify lead-like molecules and offers the structural information needed for later stages of the drug design process. The present work describes the expression, purification, and crystallization of sVP40 in a highly reproducible manner, as well as the establishment of a high-content crystallographic screening pipeline. Such identified binders usually exhibit low affinities in the high μM or low mM range, suggesting that these hits would be missed in a less stringent assay. Crystal soaking offers the additional advantage of structural information, facilitating the fragment extension process. This method is particularly suited for nonenzymatic proteins, where, like in the case of VP40, their functionality can only be assessed in cell culture-based assays involving the presence of numerous other proteins. Using fragment-based lead discovery, we identified the small-molecule SA, which binds to residues L158 of the NTD and R214 of the CTD of VP40, thereby bridging both domains. Since the flexibility of the protein is needed for membrane binding and octamerization, it is presumed that a derivative with a higher binding affinity than SA could effectively impair the protein's conformational dynamics and inhibit its functions.

It is therefore presumed that SA is a promising lead-like molecule for the development of a VP40 inhibitor. In further studies, extended derivatives of SA will be synthesized to increase the molecule's affinity for the binding pocket of sVP40. The present study offers novel perspectives on identifying small molecules that exploit vulnerable sites in a viral target protein and pave the way for potent and highly specific inhibitors.

5. METHODS

5.1. Compounds. The crystallographic screening library was provided by G.K. and A.H. in collaboration with Jena Bioscience. Salicylic acid was purchased from Thermo Fisher Scientific and Acros Organics with a purity of >95% assessed via titration assay.

5.2. Expression, Purification, and Crystallization. SUDV VP40 constructs lacking the first 43 amino acids

https://doi.org/10.1021/acsomega.4c04829
ACS Omega 2024, 9, 33193−33203

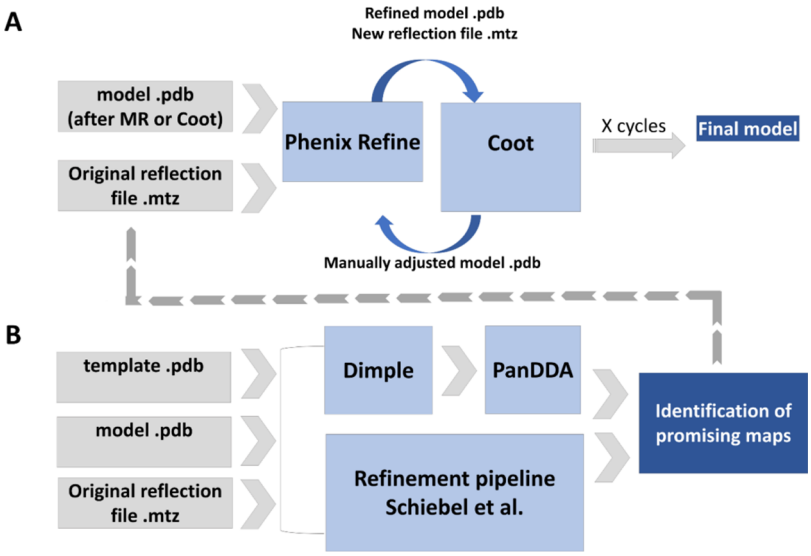

Figure 4. Workflow for the analysis of crystallographic data. (A) Promising data sets were refined using *Phenix* and *Coot* until the final model was generated. (B) Interesting data sets were identified by using both the refinement pipeline by Schiebel et al. as well as *dimple* and *PanDDA*.

($sVP40_{\Delta 43}$) were cloned into the bacterial expression plasmid pET46 and transformed into Rosetta2 cells. Expression, purification, and crystallization were performed as previously described.[26] Briefly, cells were grown in Luria−Bertani (LB) medium and induced with 0.5 mM IPTG once the exponential phase was reached ($OD_{600} \geq 0.5$). sVP40 was then expressed overnight at room temperature, bacterial cells were eventually harvested, the bacterial pellet was resuspended in VP40 buffer (25 mM Tris, 300 mM NaCl, pH 8) with 10 mM imidazole, lysed using a microfluidizer, and the supernatant was subjected to centrifugation. $sVP40_{\Delta 43}$ (WT or mutants thereof) was then purified by immobilized metal affinity chromatography using Ni-NTA beads and eluted by application of 250 mM imidazole in VP40 buffer after extensive washing steps of the beads using VP40 buffer with 20 mM imidazole. VP40-containing fractions were then applied to a HiLoad16/60 size-exclusion chromatography column using VP40 buffer as the running buffer. The total yield of the purified protein was applied to the SEC column. Eluted fractions corresponding to dimeric VP40 were collected and concentrated to 7 mg/mL $sVP40_{\Delta 43}$ in 25 mM Tris and 300 mM NaCl, pH 8, and was mixed 1:1 with crystallization buffer (100 mM *N*-(2-hydroxyethyl)piperazine-*N*′-ethanesulfonic acid (HEPES), 40 mM $MgCl_2$, 10% v/v PEG400). Crystals were grown overnight at 18 °C using the hanging drop method. As a cryoprotectant, 20% ethylene glycol was added to the crystallization buffer.

5.3. Soaking of sVP40 Crystals and Analysis. Fragments originating from the FragXtal Screen (Jena Biosciences) were dissolved in DMSO to 1 M and diluted 1:10 in crystallization buffer (with or without 20% ethylene glycol as a cryoprotectant) to a final concentration of 100 mM. Crystals were then placed in a drop of the diluted fragments and soaked for only seconds, minutes, 1 h, or overnight. Crystals were then harvested, flash-frozen in liquid nitrogen, and analyzed at the Swiss Light Source, Paul Scherrer Institute, Villigen, Switzerland. Data sets were collected and processed using *XDS*[69] and scaled using the *ccp4i* suite *Aimless*.[70] Data sets were then analyzed using the software packages *dimple*[71] and eventually *PanDDA*.[35] In addition to *PanDDA*, the autorefinement pipeline by Schiebel et al.[30] was used. For further manual evaluation, molecular replacement (MR) was performed using Phaser[72] with 4LD8[8] as a search model, and data sets were refined using iterative cycles of refinement procedures using *Phenix Refine*[73] and model building in *coot*.[74] Restraints for SA were generated using phenix-elbow. Water molecules were added manually to the model (in *coot*), which was refined for atom occupancies, individual B-factors, and TLS groups (as determined using the *Phenix* TLS tool). The overview of the crystal data analysis is given in Figure 4.

5.4. Thermal Shift Assay. For this assay, 20 μM $sVP40_{\Delta 43}$ WT in 25 mM Tris, 300 mM NaCl, pH 8, was mixed with SYPRO Orange (50× final concentration), 2 μL sodium salt (SA) was dissolved in VP40 buffer to final concentrations of 1−100 mM and VP40 buffer ad 20 μL. A melting curve analysis using a StepOne Real-Time PCR system, with the temperature ranging from 25 to 99 °C with a continuous increase of 0.05 °C/s, was performed. Each reaction was measured in triplicates, and 20 μL of each mixture was used per well of a 96-well plate. Negative controls included samples without protein or without SA.

5.54. Mutagenesis of Plasmids. Mutagenesis of sVP40 in the eukaryotic plasmid pCAGGS or the bacterial expression plasmid pET46 EK/LIC was performed using the Agilent Quickchange Lightning Mutagenesis Kit according to manufacturer's instructions. Primer sequences were as follows: ggtagcacaaactcttgagcgaaagcctggttccccat (for both pCAGGS and pET46 sVP40 L158A), tggaagtagaacgggtctcgcctttgggtgaaatgaaagc and ctctcatttcacccgaacgcgagacccgttctacttcc (for pCAGGS and pET46 sVP40 L213A, respectively), and cctggaagtagaacgggtgccagctttgggtgaaaatga and tcatttcaccaaagctggcacccgttctacttccagg (for pCAGGS and pET46 sVP40 R214A, respectively).

5.6. Mammalian Cells. HEK293 (human embryonic kidney) and HuH7 (human hepatoma) cells were maintained in Dulbecco's modified Eagle's medium (DMEM, Invitrogen) supplemented with 10% fetal calf serum (FCS), 2 mM L-glutamine (Q), 100 U/mL penicillin, and 100 μg/mL streptomycin (P/S) and grown at 37 °C and 5% CO_2.

5.7. Minigenome Assay. The principle and plasmids of minigenome (MG) assays were already described elsewhere.[38]

https://doi.org/10.1021/acsomega.4c04829
ACS Omega 2024, 9, 33193−33203

In short, HEK293 cells in 12-well plates at approximately 50% confluency were transfected with plasmids coding for the various viral proteins: 500 ng of pCAGGS L, 62.5 ng of pCAGGS VP35, 50 ng of pCAGGS VP30, 62.5 ng of pCAGGS NP, 125 ng of pCAGGS T7, 125 ng of pANDY 3E5E, 50 ng of pGL4 Firefly Luciferase, and 400 ng of pCAGGS sVP40 WT/mutants using the TransIT transfection reagent.[26] Differences in the absolute amount of transfected plasmid DNA were compensated for by the addition of an empty pCAGGS vector. For the treatment with SA, the cell culture medium was changed to 2 mL of DMEM with 3% FCS + Q/P/S with 2 μL of SA (salicylic acid sodium salt, final concentrations of 1 μM−1 mM). While we did not control for the cellular uptake of SA, several publications report a successful treatment of HEK293 cells with SA,[75−78] indicating sufficient membrane permeability. Forty-eight hours post-transfection (p.t.), cells were washed twice with PBS_{def} and eventually resuspended 1× Lysis Juice (Promega) and frozen at −20 °C. After thawing, the cell suspension was centrifuged for 10 min at 13,200 rpm and 4 °C. The supernatant was used to measure reporter gene (Renilla luciferase) activity using the Beetle-Juice and Renilla-Juice BIG KITs (PJK) with a Centro LB 960 luminometer (Berthold Technologies). Firefly luciferase signals were used to normalize the transfection efficiency. Data was analyzed using one-way analysis of variance (ANOVA) by Prism version 8.1.1 (GraphPad Software Inc., San Diego, CA).

5.8. VLP Assay. HEK293 cells in 6-well plates at approximately 50% confluency were transfected with 500 ng of pCAGGS sVP40 WT or mutants and pCAGGS EBOV GP, the latter to improve yields of virus-like particles (VLPs)[79] (3 wells per sample). Four hour p.t., the cell culture medium was changed to 3 mL of DMEM with 3% FCS + Q/P/S (for SA experiments: addition of 0.1% SA (sodium salt) with final concentrations of 1 μM−1 mM). Cell culture supernatants were collected for 24 h p.t., centrifuged for 10 min at 2500 rpm and 4 °C to remove cell debris, and the supernatant was later subjected to ultracentrifugation for 2 h at 4 °C and 40,000 rpm over a 20% sucrose cushion. Pellets containing VLPs were then resuspended in 50 μL of 1× sample buffer with β-mercaptoethanol and heated for 5 min at 95 °C. Cells were washed twice with PBS_{def} and eventually resuspended in 1× Lysis Juice (Promega) and frozen at −20 °C. After thawing, the cell suspension was centrifuged for 10 min at 13,200 rpm and 4 °C. Sixty microliter portion of the supernatants of the lysate was then mixed with 20 μL of 4× sample buffer and then treated as described for the VLP samples above. Western Blot analyses of both cell lysate and VLP samples were performed as described in the next section.

5.9. Western Blot Analysis. Protein samples were separated on a 12% sodium dodecyl sulphate (SDS)-polyacrylamide gel (50 min at 200 V) and transferred to a 0.45 μM nitrocellulose membrane (Amersham) by applying 25 V and 1 A for 30 min. The membrane was blocked using 10% skim milk in PBS_{def}, stained with rabbit α-sVP40 and mouse α-tubulin (1:1000 in 1% skim milk, diluted in PBS_{def} with 0.1% Tween-20) as primary antibodies and donkey α-mouse IRDye 680, goat α-mouse IRDye 800, and goat α-rabbit IRDye 680 using the Odyssey CLx imaging system. Signals were quantified using an Odyssey Infrared Imaging Scanner with the ImageStudio Acquisition software. Intensities of released VLP were normalized to the respective lysate samples via quantification of both VP40-specific bands. Data was analyzed using one-way ANOVA by Prism version 8.1.1 (GraphPad software Inc., San Diego, CA).

5.10. Infection of HuH7 Cells with SUDV. All infection experiments using the Sudan virus (SUDV) were performed in the BSL4 laboratory of the Institute for Virology, University of Marburg, according to national and international regulations.

HuH7 cells were seeded in 12-well plates to a confluency of 50% and infected with SUDV at an MOI of 0.1 $TCID_{50}$/mL. The required virus volume was mixed with 500 μL DMEM without FCS and added to the cells. The inoculum was removed after 1 h at 37 °C and 5% CO_2, the cells were washed thrice with PBS_{def}, and 1 mL of DMEM with 3% FCS and 0.1% DMSO/SA was added to the cells. The addition of SA was only performed once directly after infection. Two days postinfection (dpi), supernatants were harvested, and viral titers ($TCID_{50}$/mL) were assessed via the TCID50 method using the Spearman & Kärber algorithm.[80]

■ ASSOCIATED CONTENT

Supporting Information

The Supporting Information is available free of charge at https://pubs.acs.org/doi/10.1021/acsomega.4c04829.

Sequence alignment of the different ebolavirus species (Figure S1); alignment of VP40 models of different ebolavirus species (Figure S2); alignment of apo and bound structures of VP40 (Figure S3); thermal shift analysis of $sVP40_{\Delta 43}$ WT with and without SA in varying concentrations (Figure S4); comparison of eVP40 and sVP40 WT in an EBOV-based MG assay (Figure S5); representative Western blot of a R214 mutant VLP assay (Figure S6); crystal packing of $sVP40_{\Delta 43}$ WT in complex with SA (Figure S7); fragments of the Jena FragXtal Screen with similar building blocks compared to salicylic acid (Table S1) (PDF)

■ AUTHOR INFORMATION

Corresponding Author

Stephan Becker − *Institute for Virology, University of Marburg, D-35043 Marburg, Hessen, Germany; Partnersite Giessen-Marburg-Langen, German Centre for Infection Research, D-35043 Marburg, Hessen, Germany;* orcid.org/0000-0002-6621-9350; Email: becker@staff.uni-marburg.de

Authors

Anke-Dorothee Werner − *Institute for Virology, University of Marburg, D-35043 Marburg, Hessen, Germany;* orcid.org/0000-0002-9316-0227

Nils Krapoth − *Institute for Virology, University of Marburg, D-35043 Marburg, Hessen, Germany; Institut für Molekulare Biologie gGmbH, D-55128 Mainz, Rheinland-Pfalz, Germany*

Michael J. Norris − *Department of Biochemistry, University of Toronto, Toronto, Ontario M5S 1A1, Canada;* orcid.org/0000-0002-8325-5257

Andreas Heine − *Institute of Pharmaceutical Chemistry, University of Marburg, D-35032 Marburg, Hessen, Germany*

Gerhard Klebe − *Institute of Pharmaceutical Chemistry, University of Marburg, D-35032 Marburg, Hessen, Germany*

Erica Ollmann Saphire − *La Jolla Institute for Immunology, La Jolla, California 92037-1387, United States*

Complete contact information is available at:

https://doi.org/10.1021/acsomega.4c04829
ACS Omega 2024, 9, 33193−33203

https://pubs.acs.org/10.1021/acsomega.4c04829

Author Contributions

Conceptualization: A.-D.W., S.B., A.H., and G.K. Data curation: A.-D.W., Formal Analysis: A.-D.W. and M.J.N., Funding acquisition: S.B., A.H., and G.K. Investigation: A.-D.W., N.K., and M.J.N. Methodology: A.-D.W. and S.B. Project administration: A.-D.W. and S.B. Supervision: S.B., A.-D.W., and E.O.S. Visualization: A.-D.W. Writing—original draft: A.-D.W. and S.B. Writing—review and editing: A.-D.W., N.K., M.J.N., G.K., A.H., E.O.S., and S.B.

Notes

Inclusion and Diversity One or more of the authors of this paper self-identifies as a gender minority in their field of research. We support inclusive, diverse, and equitable conduct of research.

The authors declare no competing financial interest.

■ ACKNOWLEDGMENTS

The authors would like to thank Astrid Herwig for excellent technical support and the BSL4 staff at the Institute for Virology in Marburg. The authors would also like to thank the following groups of the University of Marburg, Germany: the Essen lab with Prof. Lars-Oliver Essen, Dr. Viktoria Reithofer, Dr. Laura Werel, Dr. Lukas Korf, Dr. Maximilian Biermeier, and Dr. Hans-Joachim Emmerich for their great support regarding crystal data collection at the Swiss Light Source of the Paul-Scherrer Institute in Villigen, Switzerland; Dr. Alexander Metz (Institute for Pharmaceutical Chemistry) and Dr. Jan Wollenhaupt (Helmholtz-Zentrum Berlin) for advice regarding the handling of the library; the Bange Lab with Prof. Gert Bange and Dr. Nils Maisch for their kind permission to use the microfluidizer; and the Schnare lab with Prof. Markus Schnare for the support regarding the FPLC system. This project is funded by the State of Hesse, LOEWE Center "DRUID" (Novel Drug Targets against Poverty-Related and Neglected Tropical Infectious Diseases), project A1 and A4, as well as the Network of University Medicine, Project COVIM 2 (01KX2121). Coordinates and Structure Factors have been deposited in the Protein Data Bank under accession codes 8B2U (soaking complex with SA) and 8B1S (cocrystallization complex with SA). Mtz files of the 140 data sets are deposited in the research data repository of the University of Marburg data_UMR (https://data.uni-marburg.de/collections/e84bb245-bb92-4abf-a6be-9522f6bace04).

■ ABBREVIATIONS

SUDV, Sudan virus; EBOV, Ebola virus; L domains, late budding domain; FBDD, Fragment-based drug design; or FBLD, fragment-based lead design; Ro3, Astex rule of three; Ro5, Lipinski's rule of five; SA, salicylic acid; MG, minigenome; VLP, virus-like particle; TSA, thermal shift assay

■ REFERENCES

(1) Biedenkopf, N.; Bukreyev, A.; Chandran, K.; et al. Renaming of genera Ebolavirus and Marburgvirus to Orthoebolavirus and Orthomarburgvirus, respectively, and introduction of binomial species names within family Filoviridae. *Arch. Virol.* **2023**, *168*, No. 220, DOI: 10.1007/s00705-023-05834-2.

(2) Yamaoka, S.; Ebihara, H. Pathogenicity and Virulence of Ebolaviruses with Species- and Variant-specificity. *Virulence* **2021**, *12*, 885−901.

(3) Tshiani Mbaya, O.; Mukumbayi, P.; Mulangu, S. Review: Insights on Current FDA-Approved Monoclonal Antibodies Against Ebola Virus Infection. *Front. Immunol.* **2021**, *12*, No. 721328.

(4) Woolsey, C.; Geisbert, T. W.; Dutch, R. E. Current state of Ebola virus vaccines. *PLoS Pathog.* **2021**, *17*, No. e1010078.

(5) Marzi, A.; Fletcher, P.; Feldmann, F.; et al. Species-specific immunogenicity and protective efficacy of a vesicular stomatitis virus-based Sudan virus vaccine: a challenge study in macaques. *Lancet Microbe* **2023**, *4*, e171−e178.

(6) Bwire, G.; Sartorius, B.; Guerin, P.; et al. Sudan Ebola virus (SUDV) outbreak in Uganda, 2022: lessons learnt and future priorities for sub-Saharan Africa. *BMC Med.* **2023**, *21*, No. 144, DOI: 10.1186/s12916-023-02847-1.

(7) Ibrahim, S. K.; Ndwandwe, D. E.; Thomas, K.; Sigfrid, L.; Norton, A. Sudan virus disease outbreak in Uganda: urgent research gaps. *BMJ Global Health* **2022**, *7*, No. e010982, DOI: 10.1136/bmjgh-2022-010982.

(8) Bornholdt, Z. A.; Noda, T.; Abelson, D.; et al. Structural rearrangement of ebola virus VP40 begets multiple functions in the virus life cycle. *Cell* **2013**, *154*, 763−774.

(9) Dessen, A.; Volchkov, V.; Dolnik, O.; Klenk, H. D.; Weissenhorn, W. Crystal structure of the matrix protein VP40 from Ebola virus. *EMBO J.* **2000**, *19*, 4228−4236.

(10) Ruigrok, R. W.; Schoehn, G.; Dessen, A.; et al. Structural characterization and membrane binding properties of the matrix protein VP40 of Ebola virus. *J. Mol. Biol.* **2000**, *300*, 103−112.

(11) Kolesnikova, L.; Berghöfer, B.; Bamberg, S.; Becker, S. Multivesicular bodies as a platform for formation of the Marburg virus envelope. *J. Virol.* **2004**, *78*, 12277−12287.

(12) Adu-Gyamfi, E.; Johnson, K. A.; Fraser, M. E.; et al. Host Cell Plasma Membrane Phosphatidylserine Regulates the Assembly and Budding of Ebola Virus. *J. Virol.* **2015**, *89*, 9440−9453.

(13) Yamayoshi, S.; Noda, T.; Ebihara, H.; et al. Ebola virus matrix protein VP40 uses the COPII transport system for its intracellular transport. *Cell Host Microbe* **2008**, *3*, 168−177.

(14) Hartlieb, B.; Weissenhorn, W. Filovirus assembly and budding. *Virology* **2006**, *344*, 64−70.

(15) Gomis-Rüth, F.; Dessen, A.; Timmins, J.; et al. The matrix protein VP40 from Ebola virus octamerizes into pore-like structures with specific RNA binding properties. *Structure* **2003**, *11*, 423−433.

(16) Landeras-Bueno, S.; Wasserman, H.; Oliveira, G.; et al. Cellular mRNA triggers structural transformation of Ebola virus matrix protein VP40 to its essential regulatory form. *Cell Rep.* **2021**, *35*, No. 108986.

(17) Hoenen, T.; Volchkov, V.; Kolesnikova, L.; et al. VP40 octamers are essential for Ebola virus replication. *J. Virol.* **2005**, *79*, 1898−1905.

(18) Hoenen, T.; Biedenkopf, N.; Zielecki, F.; et al. Oligomerization of Ebola virus VP40 is essential for particle morphogenesis and regulation of viral transcription. *J. Virol.* **2010**, *84*, 7053−7063.

(19) Bennett, R. P.; Finch, C. L.; Postnikova, E. N.; et al. A Novel Ebola Virus VP40 Matrix Protein-Based Screening for Identification of Novel Candidate Medical Countermeasures. *Viruses* **2021**, *13*, No. 52, DOI: 10.3390/v13010052.

(20) Urata, S.; Omotuyi, O. I.; Izumisawa, A.; et al. Identification of novel chemical compounds targeting filovirus VP40-mediated particle production. *Antiviral Res.* **2022**, *199*, No. 105267, DOI: 10.1016/j.antiviral.2022.105267.

(21) Loughran, H. M.; Han, Z.; Wrobel, J. E.; et al. Quinoxaline-based inhibitors of Ebola and Marburg VP40 egress. *Bioorg. Med. Chem. Lett.* **2016**, *26*, 3429−3435.

(22) Okumura, A.; Pitha, P. M.; Harty, R. N. ISG15 inhibits Ebola VP40 VLP budding in an L-domain-dependent manner by blocking Nedd4 ligase activity. *Proc. Natl. Acad. Sci. U.S.A.* **2008**, *105*, 3974−3979.

(23) Kirsch, P.; Hartman, A. M.; Hirsch, A. K. H.; Empting, M. Concepts and Core Principles of Fragment-Based Drug Design. *Molecules* **2019**, *24*, No. 4309, DOI: 10.3390/molecules24234309.

(24) Maveyraud, L.; Mourey, L. Protein X-ray Crystallography and Drug Discovery. *Molecules* **2020**, *25*, No. 1030, DOI: 10.3390/molecules25051030.
(25) Patel, D.; Bauman, J. D.; Arnold, E. Advantages of Crystallographic Fragment Screening: Functional and Mechanistic Insights from a Powerful Platform for Efficient Drug Discovery. *Prog. Biophys. Mol. Biol.* **2014**, *116*, 92−100.
(26) Werner, A.-D.; Schauflinger, M.; Norris, M. J.; et al. The C-terminus of Sudan ebolavirus VP40 contains a functionally important CXnC motif, a target for redox modifications. *Structure* **2023**, *31*, 1038.
(27) Gárdonyi, M.; Hasewinkel, C.; Wallbaum, J.; et al. Crystallographic Fragment Screening on the Shigella Type III Secretion System Chaperone IpgC. *ACS Omega* **2023**, *8*, 46051−46065.
(28) Hassaan, E.; Eriksson, P.-O.; Geschwindner, S.; Heine, A.; Klebe, G. Fragments as Novel Starting Points for tRNA-Guanine Transglycosylase Inhibitors Found by Alternative Screening Strategies. *ChemMedChem* **2020**, *15*, 324−337.
(29) Huschmann, F. U.; Linnik, J.; Sparta, K.; et al. Structures of endothiapepsin-fragment complexes from crystallographic fragment screening using a novel, diverse and affordable 96-compound fragment library. *Acta Crystallogr., Sect. F: Struct. Biol. Commun.* **2016**, *72*, 346−355.
(30) Schiebel, J.; Krimmer, S.; Röwer, K.; et al. High-Throughput Crystallography: Reliable and Efficient Identification of Fragment Hits. *Structure* **2016**, *24*, 1398−1409.
(31) Lipinski, C. A.; Lombardo, F.; Dominy, B. W.; Feeney, P. J. Experimental and computational approaches to estimate solubility and permeability in drug discovery and development settings. *Adv. Drug Delivery Rev.* **2001**, *46*, 3−26.
(32) Congreve, M.; Carr, R.; Murray, C.; Jhoti, H. A 'Rule of Three' for fragment-based lead discovery? *Drug Discovery Today* **2003**, *8*, 876−877.
(33) Lima, G. M. A.; Talibov, V. O.; Jagudin, E.; et al. FragMAX: the fragment-screening platform at the MAX IV Laboratory. *Acta Crystallogr., Sect. D: Struct. Biol.* **2020**, *76*, 771−777.
(34) Švecová, L.; Østergaard, L. H.; Skálová, T.; et al. Crystallographic fragment screening-based study of a novel FAD-dependent oxidoreductase from Chaetomium thermophilum. *Acta Crystallogr., Sect. D: Struct. Biol.* **2021**, *77*, 755−775.
(35) Pearce, N. M.; Krojer, T.; Bradley, A. R.; et al. A multi-crystal method for extracting obscured crystallographic states from conventionally uninterpretable electron density. *Nat. Commun.* **2017**, *8*, No. 15123.
(36) Ehrmann, F. R.; Stojko, J.; Metz, A.; et al. Soaking suggests ″alternative facts″: Only co-crystallization discloses major ligand-induced interface rearrangements of a homodimeric tRNA-binding protein indicating a novel mode-of-inhibition. *PLoS One* **2017**, *12*, No. e0175723.
(37) Wienen-Schmidt, B.; Oebbeke, M.; Ngo, K.; Heine, A.; Klebe, G. Two Methods, One Goal: Structural Differences between Cocrystallization and Crystal Soaking to Discover Ligand Binding Poses. *ChemMedChem* **2021**, *16*, 292−300.
(38) Hoenen, T.; Groseth, A.; de Kok-Mercado, F.; Kuhn, J. H.; Wahl-Jensen, V. Minigenomes, transcription and replication competent virus-like particles and beyond. *Antiviral Res.* **2011**, *91*, 195−208.
(39) McCarthy, S. E.; Johnson, R. F.; Zhang, Y.-A.; Sunyer, J. O.; Harty, R. N. Role for amino acids 212KLR214 of Ebola virus VP40 in assembly and budding. *J. Virol.* **2007**, *81*, 11452−11460.
(40) Adu-Gyamfi, E.; et al. The Ebola virus matrix protein penetrates into the plasma membrane: a key step in viral protein 40 (VP40) oligomerization and viral egress. *J. Biol. Chem.* **2013**, *288*, 5779−5789.
(41) Motsa, B. B.; Sharma, T.; Ciofi, M.; Chapagain, P. P.; Stahelin, R. V. Minor electrostatic changes robustly increase VP40 membrane binding, assembly, and budding of Ebola virus matrix protein derived virus-like particles. *J. Biol. Chem.* **2024**, *300*, No. 107213.
(42) Glöckner, S.; Heine, A.; Klebe, G. A Proof-of-Concept Fragment Screening of a Hit-Validated 96-Compounds Library against Human Carbonic Anhydrase II. *Biomolecules* **2020**, *10*, No. 518, DOI: 10.3390/biom10040518.
(43) Zhu, L.; Yang, F.; Chen, L.; Meehan, E. J.; Huang, M. Human serum albumin complexed with myristate, 3′-azido-3′-deoxythymidine (AZT) and salicylic acid,**2008**.
(44) Bavi, N. et al. Cryo-EM Structure of dolphin Prestin: Inhibited II (Sulfate + Salicylate) state, **2021**.
(45) Filippakopoulos, P. et al. Crystal Structure of the fifth bromodomain of human PB1 in complex with salicylic acid, **2015**.
(46) Gavira, J. A.; Mantilla, M. A.; Fernandez, M.; Krell, T. Ligand binding domain of the P. putida receptor PcaY_PP in complex with salicylic acid, **2020**.
(47) Mori, M.; Villa, S.; Meneghetti, F.; Bellinzoni, M. M. tuberculosis salicylate synthase MbtI in complex with salicylate and Mg2+, **2020**.
(48) Morimoto, Y.; Uemura, T. et al. Salicylate hydroxylase substrate complex. **2015**, *469*. DOI: 10.1016/j.bbrc.2015.11.087.
(49) Roske, Y. et al. Structural versatility of TasA in B. subtilis biofilm formation, **2018**.
(50) Walton, W. G.; Redinbo, M. R.; Dangl, J. L. Crystal structure of the MarR family transcriptional regulator from Variovorax paradoxus bound to Salicylic acid, **2021**.
(51) Wang, J. L.; Wang, Z. J. Pyochelin synthetase, a dimeric nonribosomal peptide synthetase elongation module-after-condensation, **2021**.
(52) Wang, W.; Withers, J.; Li, H.; et al. Structural Basis of Salicylic Acid Perception by Arabidopsis NPR Proteins. *Nature* **2020**, *586*, 311−316, DOI: 10.1038/s41586-020-2596-y.
(53) Bertoletti, N.; Marchais-Oberwinkler, S.; Heine, A.; Klebe, G. 17beta-hydroxysteroid dehydrogenase 14 variant T205 in complex with Salicylic acid, **2018**.
(54) Correy, G. J.; Young, I. D.; Thompson, M. C.; Fraser, J. S. PanDDA analysis group deposition -- Crystal structure of SARS-CoV-2 NSP3 macrodomain in complex with ZINC000000000922, **2020**.
(55) Cimmperman, P.; Baranauskienė, L.; Jachimovičiūtė, S.; et al. A quantitative model of thermal stabilization and destabilization of proteins by ligands. *Biophys. J.* **2008**, *95*, 3222−3231.
(56) Maji, B.; Gangopadhyay, S. A.; Lee, M.; et al. A High-Throughput Platform to Identify Small-Molecule Inhibitors of CRISPR-Cas9. *Cell* **2019**, *177*, 1067−1079.e19.
(57) Bhusal, R. P.; Patel, K.; Kwai, B. X. C.; et al. Development of NMR and thermal shift assays for the evaluation of Mycobacterium tuberculosis isocitrate lyase inhibitors. *MedChemComm* **2017**, *8*, 2155−2163.
(58) Nanbo, A.; Maruyama, J.; Imai, M.; et al. Ebola virus requires a host scramblase for externalization of phosphatidylserine on the surface of viral particles. *PLoS Pathog.* **2018**, *14*, No. e1006848.
(59) Mirdita, M.; Schütze, K.; Moriwaki, Y.; et al. ColabFold: making protein folding accessible to all. *Nat. Methods* **2022**, *19*, 679−682.
(60) Wu, L.; Jin, D.; Wang, D.; et al. The two-stage interaction of Ebola virus VP40 with nucleoprotein results in a switch from viral RNA synthesis to virion assembly/budding. *Protein Cell* **2022**, *13*, 120−140.
(61) Urata, S.; Ishikawa, T.; Yasuda, J. Roles of YIGL sequence of Ebola virus VP40 on genome replication and particle production. *J. Gen. Virol.* **2019**, *100*, 1099−1111.
(62) Ma, Y.-H.; Hong, X.; Wu, F.; et al. Inhibiting the transcription and replication of Ebola viruses by disrupting the nucleoprotein and VP30 protein interaction with small molecules. *Acta Pharmacol. Sin.* **2023**, *44*, 1487−1499.
(63) Luthra, P.; Anantpadma, M.; De, S.; et al. High-Throughput Screening Assay to Identify Small Molecule Inhibitors of Marburg Virus VP40 Protein. *ACS Infect. Dis.* **2020**, *6*, 2783−2799.
(64) Vanmechelen, B.; Stroobants, J.; Chiu, W.; et al. Development and optimization of biologically contained Marburg virus for high-throughput antiviral screening. *Antiviral Res.* **2022**, *207*, No. 105426.

https://doi.org/10.1021/acsomega.4c04829
ACS Omega 2024, 9, 33193−33203

(65) Anantpadma, M.; Kouznetsova, J.; Wang, H.; et al. Large-Scale Screening and Identification of Novel Ebola Virus and Marburg Virus Entry Inhibitors. *Antimicrob. Agents Chemother.* **2016**, *60*, 4471−4481.
(66) Hughes, J. P.; Rees, S.; Kalindjian, S. B.; Philpott, K. L. Principles of early drug discovery. *Br. J. Pharmacol.* **2011**, *162*, 1239−1249.
(67) Erlanson, D. A. Introduction to fragment-based drug discovery. *Top. Curr. Chem.* **2012**, *317*, 1−32.
(68) Feyfant, E.; Cross, J. B.; Paris, K.; Tsao, D. H. H. Fragment-based drug design. *Methods Mol. Biol.* **2011**, *685*, 241−252.
(69) Kabsch, W. XDS. *Acta Crystallogr., Sect. D: Biol. Crystallogr.* **2010**, *66*, 125−132.
(70) Evans, P. R. An introduction to data reduction: space-group determination, scaling and intensity statistics. *Acta Crystallogr., Sect. D: Biol. Crystallogr.* **2011**, *67*, 282−292.
(71) Wojdyr, M.; Keegan, R.; Winter, G.; Ashton, A. DIMPLE - a pipeline for the rapid generation of difference maps from protein crystals with putatively bound ligands. *Acta Crystallogr., Sect. A: Found. Crystallogr.* **2013**, *69*, s299.
(72) McCoy, A. J.; Grosse-Kunstleve, R. W.; Adams, P. D.; et al. Phaser crystallographic software. *J. Appl. Crystallogr.* **2007**, *40*, 658−674.
(73) Liebschner, D.; et al. Macromolecular structure determination using X-rays, neutrons and electrons. *Acta Crystallogr., Sect. D: Biol. Crystallogr.* **2019**, *75*, 861−877.
(74) Emsley, P.; Cowtan, K. Coot. *Acta Crystallogr., Sect. D: Biol. Crystallogr.* **2004**, *60*, 2126−2132.
(75) Sadeghi, F.; Kumar, M.; Bandey, I. N.; et al. Salicylic acid inducible nucleocytoplasmic shuttling of NPR1 fusion proteins in human cells. *Biotechnol. Bioeng.* **2022**, *119*, 199−210.
(76) Jiang, G.; Dallas-Yang, Q.; Liu, F.; Moller, D. E.; Zhang, B. B. Salicylic acid reverses phorbol 12-myristate-13-acetate (PMA)- and tumor necrosis factor alpha (TNFalpha)-induced insulin receptor substrate 1 (IRS1) serine 307 phosphorylation and insulin resistance in human embryonic kidney 293 (HEK293) cells. *J. Biol. Chem.* **2003**, *278*, 180−186.
(77) Mügge, F. L. B.; Silva, A. M. Aspirin metabolite sodium salicylate selectively inhibits transcriptional activity of ATF6α and downstream target genes. *Sci. Rep.* **2017**, *7*, No. 9190.
(78) Choi, H. W.; Tian, M.; Manohar, M.; et al. Human GAPDH Is a Target of Aspirin's Primary Metabolite Salicylic Acid and Its Derivatives. *PLoS One* **2015**, *10*, No. e0143447.
(79) Noda, T.; Sagara, H.; Suzuki, E.; et al. Ebola virus VP40 drives the formation of virus-like filamentous particles along with GP. *J. Virol.* **2002**, *76*, 4855−4865.
(80) Hierholzer, J. C.; Killington, R. A. *Virology Methods Manual, Virus isolation and Quantitation*; Elsevier, 1996.

https://doi.org/10.1021/acsomega.4c04829
ACS Omega 2024, 9, 33193−33203